Journal of Magnetism and Magnetic Materials 642 (2026) 173912

Contents lists available at ScienceDirect

Journal of Magnetism and Magnetic Materials

journal homepage: www.elsevier.com/locate/jmmm

Research article

The impact of bi-phasic crystal structure on the magnetic and transport properties of single crystalline $NdBaMn_2O_{5+\delta}$

H. Fabrelli [a], C. Macchiutti [a], J.R. Jesus [a,b], D.A. Mayoh [c], G. Balakrishnan [c], L. Bufaiçal [d], E.M. Bittar [a,*]

[a] Centro Brasileiro de Pesquisas Físicas, 22290-180, Rio de Janeiro, RJ, Brazil
[b] Universidade Federal do Rio de Janeiro, Rio de Janeiro, RJ 21941-853, Brazil
[c] Department of Physics, University of Warwick, CV4 7AL, Coventry, United Kingdom
[d] Instituto de Física, Universidade Federal de Goiás, 74001-970, Goiânia, GO, Brazil

ARTICLE INFO

Keywords:
Single crystal
Manganites
Ferromagnetism
Transport proprieties

ABSTRACT

The $LnBaMn_2O_5$ (Ln = rare-earth) manganites have attracted considerable recent interest due to their potential for use as oxygen storage materials and as solid oxide fuel cells. However, there is scarce data on the magnetic properties of some prototypical materials. Here, we report the synthesis of a single-crystalline $NdBaMn_2O_{5+\delta}$ compound by the floating-zone method and investigate its structural, electronic, and magnetic properties. The structural data indicate that, at room temperature, the material consists of a mixture of a $NdBaMn_2O_5$ phase with a layered arrangement of the Nd/Ba ions (space group $P4/nmm$) and a $NdBaMn_2O_6$ phase with a disordered distribution of Nd/Ba (space group $Imma$). Measurements of magnetization performed with the magnetic field applied at distinct crystallographic directions reveal a rich magnetic diagram, which is compared with that of similar rare-earth manganites. A peculiar anisotropy is observed between the c axis and the ab plane of the $NdBaMn_2O_5$ phase, suggesting a G-type magnetic structure in which the Mn moments are oriented along the ab planes. The electrical transport data show a pronounced magnetoresistance, which is discussed in terms of the system's crystal structure and the presence of mixed-valent Mn.

1. Introduction

The Mn-based oxides, commonly referred to as manganites, are among the most widely investigated classes of materials, exhibiting a plethora of interesting properties, including colossal magnetoresistance and multiferroism, which could be applied in magnetic storage media, magnetic sensors, and other devices [1]. From a fundamental point of view, the study of these compounds has led to the formulation of new physical concepts, such as double exchange and the Jahn-Teller polaron [2]. Recently, the interest in manganites was renewed with the discovery of a high capacity of oxygen storage on the $LnBaMn_2O_{5+\delta}$ (Ln = rare-earth) compounds, in which the reduction ($\delta = 0$) and oxidation ($\delta = 1$) processes occur efficiently and reversibly at moderate temperatures of the order of 200-500 °C, opening the path for applications [3,4]. Among these A-site layered double perovskite-type oxides, $NdBaMn_2O_{5+\delta}$ stands as presenting potential to act as a symmetrical electrode, *i.e.* it can act as both the anode and the cathode for solid oxide fuel cells, being thus advantageous in terms of device fabrication and operation [5,6].

In the $LnBaMn_2O_{5+\delta}$ perovskites, the rare-earth's magnetic moment and ionic radius are determinant for the system's physical properties. For instance, the increased A-site average radius in $GdBaMn_2O_5$ gives rise to a layered and charge-ordered compound presenting antiferromagnetic (AFM) coupling between Mn^{3+} and Mn^{2+}. At the same time, Gd^{3+} couples ferromagnetically (FM) with Mn^{3+} at low temperatures, resulting in an unusual ferrimagnetic (FIM) behavior where a magnetization reversal is observed at intermediate temperatures [7]. Conversely, $PrBaMn_2O_5$ is expected to be a half-metal exhibiting FM ordering [8]. The $NdBaMn_2O_5$ system, in turn, lies at the boundary between phases where the charge-ordered/orbital-ordered, charge-disordered/orbital-ordered, and charge-disordered/orbital-disordered phases may compete. From this, it follows that ambiguous or contradictory reports may be found in the literature regarding this compound, especially concerning its crystal structure. Early studies showed that the annealing of disordered polycrystalline $Nd_{0.5}Ba_{0.5}MnO_3$ in a reducing medium leads to the formation of A-site ordered $NdBaMn_2O_5$, which was described as belonging to the tetragonal $P4/mmm$ space group at room temperature [9,10]. Later on, $NdBaMn_2O_{5.4}$ grown in argon-flow

* Corresponding author.
E-mail address: bittar@cbpf.br (E.M. Bittar).

https://doi.org/10.1016/j.jmmm.2026.173912
Received 14 July 2025; Received in revised form 3 February 2026; Accepted 5 February 2026
Available online 6 February 2026

was described as presenting cubic $Pm\text{-}3m$ symmetry [11], while most recently a detailed examination employing neutron diffraction have shown that $NdBaMn_2O_5$ belongs to tetragonal $P4/nmm$ space group and $NdBaMn_2O_{5.5}$ presents the orthorhombic $Icma$ structure at 338 K [6]. In part, these apparently conflicting results for this compound result from the fact that the reduction/oxidation of $NdBaMn_2O_{5+\delta}$ near room temperature is accompanied by structural transition, in addition, some attempts to synthesize reduced $LnBaMn_2O_5$ in air atmosphere usually lead to the formation of concomitant secondary phases such as $LnBaMn_2O_6$ and/or $BaMnO_3$ [4–6,10,12].

The crystal structure of fully oxidized $NdBaMn_2O_6$ perovskite is also subject to controversy. The first reports describe the samples prepared by solid state reaction in argon atmosphere as presenting cubic symmetry and A-site disorder, while the annealing of the material in O_2 leads to the formation of A-site ordered phase, initially ascribed to the tetragonal $P4/mmm$ structure [9,13–15]. Later, a neutron diffraction study of an A-site disordered sample produced by sol–gel in air ascribed this compound as belonging to the orthorhombic $Imma$ space group. In contrast, the ordered phase was ascribed to the $Pmmm$ symmetry [6, 16]. At the same time, polycrystalline samples prepared by solid state reaction in air were described as belonging to triclinic $P\text{-}1$ [4] or tetragonal $P4/mmm$ [5] space groups. Recently, a polycrystal produced by solid-state reaction, but in an Ar/H_2 atmosphere, was reported to present the orthorhombic $Cmmm$ structure at room temperature, with a structural transition to the $P2_1am$ space group starting to develop at 280 K [17], whereas samples slightly doped with Cr, Co, Ni adopt the $Imma$ space group [18]. Single crystal grown by floating zone in argon followed by annealing in O_2 was also initially described as belonging to the $Cmmm$ symmetry at room temperature [19], but following studies of this same sample through electron diffraction and first principles calculations ascribed it to the $C2mm$ structure [20], and subsequently as a mixture of $C2mm$ and $Cmmm$ space groups [21].

The reports make it clear that, as with other manganites [22], the $NdBaMn_2O_{5+\delta}$ system is extremely sensitive to synthesis conditions due to its strong dependence on oxygen content [23]. Furthermore, although rare-earth manganites have been extensively investigated over the past decades, important details of their magnetic and transport properties remain lacking in the literature. For instance, the magnetic properties of single-crystalline A-site disordered $NdBaMn_2O_6$ have not been reported for temperatures below the Nd-ordering, and the magnetotransport properties of A-site ordered $NdBaMn_2O_5$ are also not available for single crystals. Also of fundamental interest is the influence of an A-site disordered phase on the anisotropies of the A-site ordered phase. In this context, we describe the synthesis of a single-crystal that presents both the ordered $NdBaMn_2O_5$ and disordered $NdBaMn_2O_6$ phases concomitantly, and investigate the impact of this bi-phasic crystal structure on the magnetic and transport properties of the system.

2. Experimental

Polycrystalline $NdBaMn_2O_{5+\delta}$ was produced by solid-state reaction. Stoichiometric amounts of Nd_2O_3, $BaCO_3$, and MnO were ground and heated in a flow of argon gas at 1000 °C (10 h), 1200 °C (12 h), and 1400 °C (12 h). The powder was then pressed into cylinders of ~7 mm diameter (up to 50 MPa) using rubber forms to serve as the feed and seed rods for the production of the single-crystal, and sintered at 1400 °C in a flow of argon for 12 h. The single crystal was produced by the floating-zone technique using a Quantum Design IR Image Furnace. The crystal was grown in air at a rate of 2.5 mm/h, with the feed and seed rods rotating in opposite directions at 20 rpm.

The crystalline structural characterization was performed using room-temperature X-ray powder diffraction (XRD) on a PANalytical Empyrean diffractometer with Cu $K_{\alpha 1,2}$ radiation. The pattern was taken over the angular range $10° \leq 2\theta \leq 100°$, with a 2θ step size of 0.013°. Rietveld refinements were performed using GSAS software and its graphical interface program [24]. X-ray Laue backscattering patterns were recorded using a commercial Photonic Science Laue System to cut and align the samples in different directions for magnetic and transport measurements. Magnetization as a function of temperature [$M(T)$] and as a function of external magnetic field [$M(H)$] curves were measured in both zero field cooled (ZFC) and field cooled (FC) modes, using a Quantum Design Physical Property Measurement System (PPMS), model Dynacool. The electrical transport data were also collected in the PPMS. The four-contact configuration was adopted, using platinum wires and silver paste for the contacts.

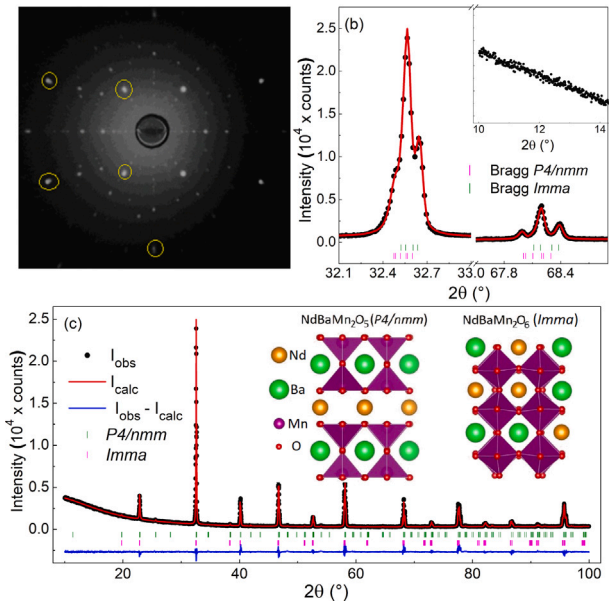

Fig. 1. (a) Laue image of the single crystal oriented along the (001) direction of the $P4/nmm$ space group. The highlighted areas, marked by yellow circles, are duplicated reflections of the pattern (see main text). (b) Magnified view of the room temperature XRD pattern encompassing Bragg reflections of the $P4/nmm$ and $Imma$ symmetries, while the inset shows the 10°-14° region. (c) Rietveld refinement fitting of the complete XRD pattern. The inset shows schematic views of the $NdBaMn_2O_5$ ($P4/nmm$) and $NdBaMn_2O_6$ ($Imma$) structures.

3. Results and discussion

Fig. 1(a) shows the Laue X-ray diffraction pattern of the synthesized crystal. The observed pattern could be indexed considering a $NdBaMn_2O_5$ structure of the $P4/nmm$ space group, oriented in the (001) direction. However, a closer inspection of the image reveals that some reflections are duplicated. These highlighted areas, marked by yellow circles, could be due to twinning or the presence of a second phase whose reflection points nearly coincide with those of the $P4/nmm$ symmetry. To unravel this issue, we performed XRD on a powdered piece of the single crystal, which revealed the presence of a secondary $NdBaMn_2O_6$ phase in the $Imma$ structure (see discussion below), giving rise to the blurred reflections indicated by the yellow circles.

From the room temperature XRD patterns, attempts to refine the material's structure as a single phase, whether $NdBaMn_2O_5$, $NdBaMn_2O_6$, or even $NdBaMn_2O_{5.5}$, did not succeed for any of the space groups previously reported for $NdBaMn_2O_{5+\delta}$ with δ ranging from 0 to 1. Conversely, a good match between experiment and simulation is achieved when a mixture of $NdBaMn_2O_5$ (hereafter called O_5) and $NdBaMn_2O_6$ (O_6) phases is considered, with the best refinement consisting of ~70% of O_5 in the $P4/nmm$ space group and ~30% of O_6 in the $Imma$ symmetry, leading to a nominally $NdBaMn_2O_{5.3}$ compound. Fig. 1(b) shows magnified views of selected reflections to highlight some

Table 1
Main results obtained from the Rietveld refinement. The numbers in parentheses correspond to the standard deviations in the last digits.

Phase	Fraction (%)	a (Å)	b (Å)	c (Å)	Mn_1–O_1 (Å)	Mn_1–O_2 (Å)	Mn_2–O_1 (Å)	Mn_2–O_2 (Å)	Mn–O_1–Mn (°)	Mn–O_2–Mn (°)	Reliability (%)
$P4/nmm$	67	5.5019(1)	5.5019(1)	7.7664(1)	2.153(3)	1.507(1)	1.703(3)	2.399(1)	180.0(0)	169.4(1)	R_{wp} = 6.2
$Imma$	33	5.5082(2)	7.7979(1)	5.5026(1)	1.956(4)	1.953(2)	1.956(4)	1.953(2)	170.3(5)	170.7(4)	R_p = 3.8

regions that could not be well fitted within a single crystallographic phase. Previous study of thermal cycles under distinct atmospheres in polycrystalline $NdBaMn_2O_{5+\delta}$ showed a complete reduction of the O_6 phase to O_5 at ~200 °C when the material is heated and cooled in air. In contrast, the presence of both O_5 and O_6 phases is observed at room temperature when it is thermal-cycled in 5% H_2/He [6]. In the case of our single-crystal, the presence of some amount of O_6 at room temperature is consistent with a scenario of incomplete oxygen reduction after the thermal cycling that occurs during the material's production at the floating zone furnace, thereby attesting that $NdBaMn_2O_{5+\delta}$ is extremely sensitive to the synthesis conditions. Here, it is worth noting that a similar level of refinement was achieved when the Nd/Ba layered $Cmmm$ space group was considered for the O_6 phase. However, as will be discussed later, the magnetic properties suggest the presence of disorder at the A-site for the O_6 phase, from which we conclude that a mixture of ordered and disordered phases is most plausible.

Fig. 1(c) shows the Rietveld refinement fitting of the complete XRD pattern as a mixture of $P4/nmm$ and $Imma$ space groups for respectively the O_5 and O_6 phases, which resulted in R_{wp} = 6.2%, R_p = 3.8% reliability factors. The main parameters obtained from the refinement are depicted in Table 1. While the $P4/nmm$ symmetry corresponds to a layered arrangement of the Nd and Ba ions, for $Imma$ the Nd and Ba share the same site, meaning a disordered distribution of these ions. The Laue pattern indicates that both phases are in the same crystallographic orientation along the crystalline rod, which significantly affects the magnetic and transport data. While the formation of Nd/Ba layers leads to a roughly bi-dimensional system on the O_5 phase, for which the most relevant magnetic couplings and electronic transport occur in-between the planes, for the disordered O_6 phase a tridimensional magnetic structure is expected. The layered Nd/Ba arrangement is expected to be manifested by the presence of a small (001) peak at ~ 11.5° in the XRD pattern. As the inset of Fig. 1(b) shows, such a peak is not clearly observed in our data. At first glance, this could be interpreted as a complete breaking of the bi-dimensional character due to a fully disordered arrangement of Nd/Ba at the A-site. However, noticeable anisotropy is observed in our magnetic and transport measurements, suggesting that some layered ordering is present. Still, the disordered O_6 phase and the background could mask its expected manifestation as a weak (001) peak. In any case, the absence of such a peak prevents a reliable estimate of the degree of Nd/Ba ordering at the A-site.

The ZFC–FC $M(T)$ measurements were performed with H = 0.01 T pointing parallel as well as perpendicular to the crystal's c axis (respectively, ∥ and ⊥ to 001). Fig. 2(a) shows an FM-like behavior for the FC curves, with a first transition at $T_C \simeq$ 131 K, followed by an anomaly at approximately 65 K. The observed magnetic irreversibility can be ascribed to domain-wall depinning, a mechanism also observed in other single-crystalline double perovskites [25]. Previous studies have shown that in the layered $NdBaMn_2O_5$ system, the Mn^{2+}–Mn^{3+} magnetic ordering starts to develop around 130 K [10,19], whereas for $NdBaMn_2O_6$ the Mn^{3+}–Mn^{4+} FM ordering is reported to occur above 235 K for the A-site ordered and below ~90 K for the A-site disordered samples [10,15,17,19,26].

In order to get a quantitative comparison between our results and previous reports for pure O_5 and O_6 phases, we show in Fig. 2(b) the plot of the average of our ∥ and ⊥ $M(T)$ together with a curve, adapted from Ref. [10], consisting of weighted contributions of pure A-site ordered O_5 and pure A-site disordered O_6 polycrystals. The curves obtained from our sample show some similarities to those reported in Ref. [10], in particular in their shapes at lower temperatures and in

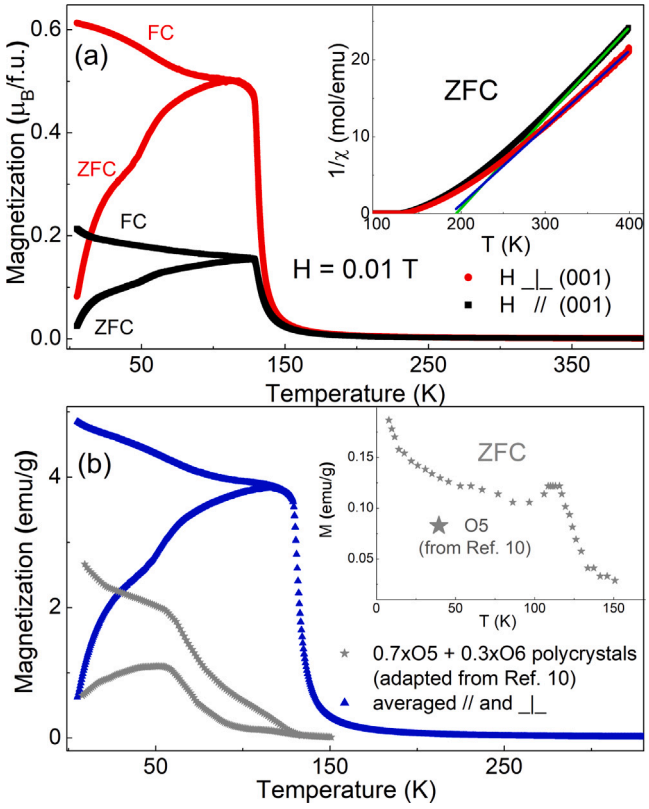

Fig. 2. (a) ZFC–FC $M(T)$ curves measured with H = 0.01 T applied along (∥) and perpendicular (⊥) to the crystal's (001) direction. The inset shows the χ^{-1} curves in the paramagnetic region, where the straight lines correspond to fits to the Curie–Weiss law. (b) Comparison between a curve produced from the averaged ∥ and ⊥ $M(T)$ curves of our sample, and a curve, adapted from Ref. [10], resulting from weighted contributions of pure A-site ordered O_5 phase (70%) and pure A-site disordered O_6 phase (30%). The inset shows a magnified view of the ZFC curve of pure A-site ordered O_5 polycrystal, extracted from Ref. [10].

the presence of two anomalies at ~130 K and ~60 K. Although the first magnetic transition is not clearly visible in the curve from the early report, the magnified ZFC curve for pure polycrystalline O_5 depicted in the inset in Fig. 2(b) attests to its presence.

One can also observe striking differences between the curves, the most notable being the magnetization magnitude, which is approximately twice as large in our sample as in the curve reported in Ref. [10]. This may be attributed to the polycrystalline nature of the sample investigated in the early report. While our sample exhibits clear signals of long-range order, the anticipated isotropic distribution of the grains' magnetic moments within the polycrystal, and the intrinsically defective and frustrated nature of their boundaries, may hinder the percolation of long-range order. Deviation from the assumed 7:3 ratio of the O5/O6 phases, as well as short-range effects at the O_5-O_6 interfaces, cannot be ruled out. Nevertheless, we can conclude that $T_C \simeq$ 131 K observed in our sample is associated with the Mn^{2+}–Mn^{3+} coupling present in the layered O_5 phase, while the second anomaly below 65 K is most likely related to the Mn^{3+}–Mn^{4+} FM coupling in the disordered O_6 phase. The presence of two magnetic transitions indicates that phase

segregation is maintained at low temperatures, *i.e.*, there is no complete reduction of the oxygen stoichiometry from O_6 to O_5. Moreover, this further suggests that the disordered O_6 phase is conducive to trapping the "excessive" oxygen ion. This finding aligns with previous studies, as oxygen redox below room temperature has not been reported for disordered $NdBaMn_2O_6$ [9,13,15,16]

Regarding the Nd^{3+} moment, there is no clear indication of its ordering down to the lowest measured temperature (5 K), signaling a decoupling of the Nd^{3+} magnetic ions from the Mn ordering, as commonly observed for rare-earth-based manganites [7,10,27,28]. In this scenario, the subtle increase in magnetization at low temperatures observed on the FC curves would be attributed to a paramagnetic component arising from Nd^{3+} moments. A more detailed investigation using element-sensitive techniques, such as X-ray magnetic circular dichroism and neutron powder diffraction, would be necessary to verify this scenario.

Importantly, the magnetization of the ⊥ to (001) curves is significantly higher than that of the ∥ to (001) ones, suggesting a larger magnetic component along the *ab* plane. Despite the recent extensive investigation of $NdBaMn_2O_{5+\delta}$ by neutron diffraction, these studies primarily focused on the redox behavior at higher temperatures, leaving the low-temperature magnetic structure undetermined. In any case, this result is at the odds with those observed for similar O_5 rare-earth-based manganites such as $GdBaMn_2O_5$, $YBaMn_2O_5$ and $SmBaMn_2O_5$, on which the Mn moments form AFM arrays aligned along the *c*-direction [7,29,30], resulting in larger magnetization along (001). Conversely, $LaBaMn_2O_{5+\delta}$ exhibits a G-type AFM ordering where the Mn spins form FM layers along the *ab* plane, with the adjacent planes being AFM coupled to each other [31]. This is in agreement with the Goodenough–Kanamori–Anderson (GKA) rules, that predict FM coupling between occupied Mn^{2+} and empty Mn^{3+} $d_{x^2-y^2}$ orbitals and AFM along *c* direction between the occupied d_{z^2} orbitals [29,32]. Here it is crucial to stress that these GKA-derived predictions are calculated for linear Mn-O-Mn bonds, *i.e.* for 180° angles. In this context, the smaller ionic radii of Sm, Gd and Y concerning that of Nd and La [33] result in more pronounced bending of the Mn-O_1–Mn angles, being this a possible reason for the breakdown of the GKA rules in the $(Gd,Sm,Y)BaMn_2O_5$ compounds.

Inset of Fig. 2(a) shows the reciprocal magnetic susceptibility (χ^{-1}) curves. A fit of the paramagnetic region of the ∥ to (001) curve within the Curie–Weiss law results in an effective magnetic moment $\mu_{eff} = 8.2$ μ_B/f.u. The paramagnetic moment expected for a system consisting of respectively ~70% and ~30% of the O_5 and O_6 phases can be computed assuming the standard values for Mn^{2+}, Mn^{3+}, Mn^{4+} and Nd^{3+} [34]

$$\mu \simeq \sqrt{0.7(\mu_{Mn^{2+}})^2 + (\mu_{Mn^{3+}})^2 + 0.3(\mu_{Mn^{4+}})^2 + (\mu_{Nd^{3+}})^2} = \sqrt{0.7(5.9)^2 + (4.9)^2 + 0.3(3.9)^2 + (3.6)^2} = 8.1\mu_B, \quad (1)$$

which is fairly close to the experimental result.

The Curie–Weiss temperature obtained from the fit is $\theta_{CW} = 194$ K. The positive value can be attributed to the FM contribution from the O_6 phase and the FM layers in the *ab* planes of the O_5 phase. Its magnitude, however, is relatively higher than T_C. In this context, it is essential to notice a significant divergence between the ∥ to (001) and the ⊥ to (001) curves, with the Curie–Weiss-fit of the latter resulting in $\theta_{CW} = 188$ K and $\mu_{eff} = 9.2$ μ_B/f.u. These discrepancies, as well as the nonlinear behavior observed for a large temperature interval above T_C, suggest deviation from the Curie–Weiss law. A possible source for this discrepancy is the low dimensionality of the O_5 phase, where the ordered Nd/Ba layers and the absence of oxygen ions linking two successive MnO_5 tetrahedra along *c* lead to a quasi-2-dimensional structure along *ab* [see the inset of Fig. 1(b)]. Furthermore, we recall that the redox of $NdBaMn_2O_{5+\delta}$ starts to develop relatively close to room temperature, altering the Mn formal valence and, consequently, its magnetic moments. Finally, as will be discussed later, our transport data indicate some degree of electron delocalization, in line with other

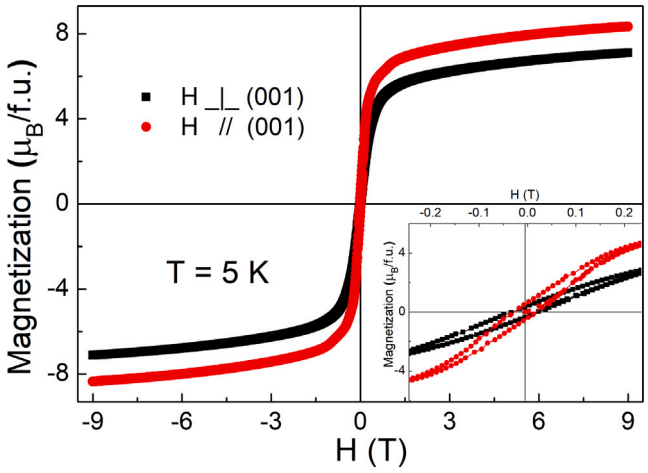

Fig. 3. ZFC $M(H)$ curves measured at 5 K with H applied ∥ and ⊥ to (001). The inset shows a magnified view of the region close to $H = 0$.

Nd-based manganites [35]. All these features are expected to contribute to deviations from Curie–Weiss behavior [36].

Fig. 3 shows the $M(H)$ measurements performed at 5 K with H applied ∥ and ⊥ to (001). The curves exhibit FM-like character and roughly the same coercive field, as highlighted in the inset [$H_C = 250$ and 220 Oe for H applied ∥ and ⊥ to (001), respectively]. However, a significant difference in the curves' magnitudes is observed at high fields. Furthermore, the saturation is incomplete even at $H = 9$ T, with a nearly linear increase in magnetization in the high-H region. The "saturation" magnetization (M_S), here approximated as the magnetization value at 9 T, cannot be explained by simple collinear FM or AFM interactions. Particularly, the $M_S = 8.3$ μ_B/f.u. obtained from the ⊥ to (001) curve can be accounted by the FM coupling between Mn^{2+} (S = 5/2) and Mn^{3+} (S = 4/2) in the O_5 phase and between Mn^{3+} and Mn^{4+} (S = 3/2) in the O_6, and assuming that the contribution from the paramagnetic Nd^{3+} is small in comparison with that of ordered Mn moments:

$$M_\perp \simeq 0.7(M_{Mn^{2+}} + M_{Mn^{3+}}) + 0.3(M_{Mn^{3+}} + M_{Mn^{4+}}) = 8.4\mu_B, \quad (2)$$

The discrepancy between the expected and observed results can be attributed to Mn^{n+}–O–Mn^{n+} AFM interactions induced by anti-site disorder, as well as to the progressive contribution of paramagnetic Nd ions. For the ∥ to (001) curve, a comparison between the $M_S = 7.1$ μ_B/f.u. experimentally observed and theoretical values are more difficult due to the H-induced inclination (canting) of the magnetic moments along *c*. In any case, the differences between the $M(H)$ curves give further evidence of a significant magnetic anisotropy in our sample.

The electrical resistivity as a function of temperature [$\rho(T)$] measurements performed with distinct H applied ∥ to (001) are displayed in Fig. 4(a). Qualitatively, the overall increase of ρ with decreasing temperature suggests an insulating- or semiconducting-like character for this system, with $\rho \simeq 0.6\Omega$·cm at room temperature for the $H = 0$ curve. However, the gentle increase of ρ with decreasing temperature down to below T_C contrasts with the logarithmic behavior usually observed in semiconducting and insulating compounds. Furthermore, fitting the high-temperature region with the power law equation of the thermally activated mechanism [inset of Fig. 4(a)] yields an activation energy, $E_G \simeq 0.1$ eV, which is smaller than the values commonly found for semiconductors. These findings, together with the apparent change in the slope of the curve around T_C, indicate a strong correlation between the magnetic and transport properties in this system, and further signal to FM couplings on Mn^{2+}–Mn^{3+} and Mn^{3+}–Mn^{4+} via

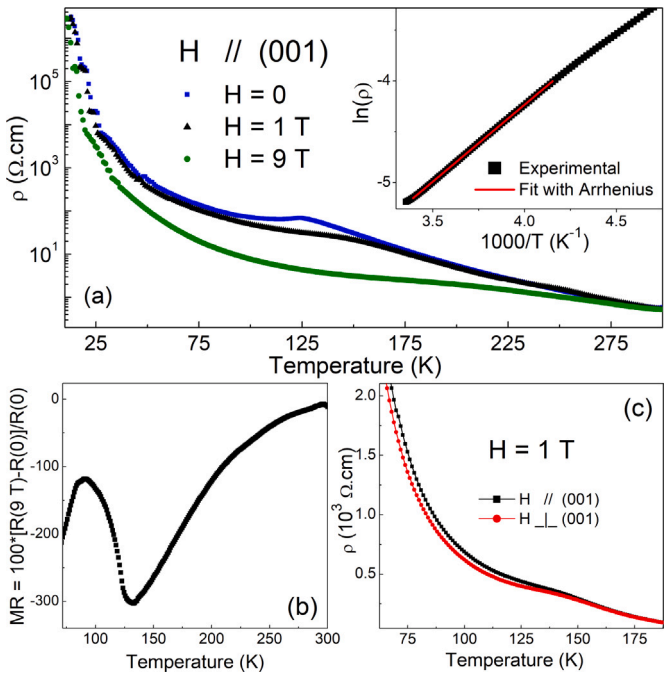

Fig. 4. (a) $\rho(T)$ measured with $H = 0$, 1 T and 9 T applied ∥ to (001). The inset shows the fit of the high-temperature region of the $H = 0$ curve with the thermally activated model. (b) MR as a function of temperature calculated from the $H = 0$ and 9 T. (c) Magnified view of the region around T_C and below of the $\rho(T)$ curves measured with $H = 1$ T applied ∥ and ⊥ to (001).

the double-exchange mechanism. At lower temperatures, a more pronounced increase of ρ is noticed, possibly associated with interdomain regions, which are known for their defective and frustrated character. Furthermore, the presence of Mn^{n+}–Mn^{n+} interactions brought by disorder may also contribute to the increase of ρ with decreasing temperature.

As Fig. 4(a) also shows, a significant magnetoresistance (MR) starts to develop as the temperature decreases, in special around and below T_C, favoring the picture of double-exchange on the Mn^{2+}–Mn^{3+} coupling, although one cannot rule out the possibility of charge-ordering on Mn ions of the O_5 phase, with the most contribution to the electrical transport coming from the Mn^{3+}–Mn^{4+} coupling of the O_6 phase. Fig. 4(b) shows the evolution of MR = 100×[$\rho(H)$ - $\rho(0)$]/$\rho(0)$ calculated from the $H = 9$ T and 0 $\rho(T)$ curves, where a maximum of the order of −300% at T_C makes of this a colossal magnetoresistive manganite [37]. Fig. 4(c) compares $\rho(T)$ curves measured with $H = 1$ T applied ∥ and ⊥ to (001). As can be seen, the curves start to bifurcate below T_C, with the ⊥ to (001) lying below the ∥ to (001) one. This provides further evidence of a G-type magnetic structure in the O_5 phase, on which the Mn spins are FM coupled along *ab*. This result also signals at least partial Nd/Ba ordering in the O_5 phase, where the Nd layers and the absence of intermediate oxygen ions linking adjacent Mn layers along the *c* axis lead to a larger resistance in this direction. Here, it is important to note that, for these measurements, the electrical field and H were not necessarily applied in the same direction. If, instead, both H and the electrical field were applied in the same direction for the ∥ and ⊥ to (001) measurements, one could expect a larger divergence between the curves.

4. Conclusion

In summary, our single-crystalline sample of $NdBaMn_2O_{5+\delta}$ synthesized by the floating zone technique is found to consist of, at room temperature, approximately 70% of a O_5 phase in the $P4/nmm$ SG, on which the Nd and Ba ions form alternating layers, and 30% of a O_6 belonging to the $Imma$ SG, where the Nd and Ba ions are disorderedly arranged at the A-site. The magnetometry measurements revealed a significant anisotropy, most likely associated with a G-type AFM magnetic structure on the Mn ions belonging to the O_5 phase, with its moments coupled FM along the *ab* planes and AFM along *c*. For the disordered O_6 phase, the expected FM coupling between Mn^{3+} and Mn^{4+} is observed. The $M(T)$ curves also evidence that the O_6 phase persists down to low temperatures. The electrical transport measurements carried out at distinct temperatures and H revealed a colossal magnetoresistance below T_C, consistent with Mn^{2+}–Mn^{3+} and Mn^{3+}–Mn^{4+} double-exchange mechanism.

CRediT authorship contribution statement

H. Fabrelli: Writing – review & editing, Investigation, Formal analysis. **C. Macchiutti:** Writing – review & editing, Investigation, Formal analysis. **J.R. Jesus:** Writing – review & editing, Investigation, Formal analysis. **D.A. Mayoh:** Writing – review & editing, Investigation, Formal analysis. **G. Balakrishnan:** Writing – review & editing, Investigation, Funding acquisition, Formal analysis. **L. Bufaiçal:** Writing – review & editing, Writing – original draft, Investigation, Formal analysis. **E.M. Bittar:** Writing – review & editing, Writing – original draft, Investigation, Formal analysis, Conceptualization.

Declaration of competing interest

The authors declare that they have no known competing financial interests or personal relationships that could have appeared to influence the work reported in this paper.

Acknowledgments

This work was supported by the Brazilian funding agencies: Fundação Carlos Chagas Filho de Amparo à Pesquisa do Estado do Rio de Janeiro (FAPERJ) [Nos. E-26/211.291/2021 and E-26/204.206/2024], Fundação de Amparo à Pesquisa do Estado de Goiás (FAPEG) and Conselho Nacional de Desenvlovimento Científico e Tecnológico (CNPq) [Nos. 305394/2023-1]. We also thank the University of Warwick International Partnership Fund for financial support for the joint collaborative project between the University of Warwick and the CBPF. The work at the University of Warwick was also supported by EPSRC, UK, through Grant EP/T005963/1.

Data availability

Data will be made available on request.

References

[1] Myron B. Salamon, Marcelo Jaime, The physics of manganites: Structure and transport, Rev. Modern Phys. 73 (2001) 583.
[2] J.M.D. Coey, M. Viret, S. von Molnár, Mixed-valence manganites, Adv. Phys. 48 (2) (1999) 167.
[3] Teruki Motohashi, Taku Ueda, Yuji Masubuchi, Makoto Takiguchi, Tohru Setoyama, Kazunori Oshima, Shinichi Kikkawa, Remarkable oxygen intake/release capability of $BaYMn_2O_{5+\delta}$: Applications to oxygen storage technologies, Chem. Mater. 22 (2010) 3192.
[4] Alicja Klimkowicz, Konrad Świerczek, Akito Takasaki, Janina Molenda, Bogdan Dabrowski, Crystal structure and oxygen storage properties of $BaYMn_2O_{5+\delta}$ (Ln: Pr, Nd, Sm, Gd, Dy, Er and Y) oxides, Mater. Res. Bull. 65 (2015) 116.
[5] Oscar L. Pineda, Zulma L. Moreno, Pascal Roussel, Konrad Świerczek, Gilles H. Gauthier, Synthesis and preliminary study of the double perovskite $NdBaMn_2O_{5+\delta}$ as symmetric SOFC electrode material, Solid State Ion. 288 (2016) 61.
[6] Florent Tonus, Mona Bahout, Vincent Dorcet, Gilles H. Gauthier, Serge Paofai, Ronald I. Smith, Stephen J. Skinner, Redox behavior of the SOFC electrode candidate $NdBaMn_2O_{5+\delta}$ investigated by high-temperature in situ neutron diffraction: first characterisation in real time of an $LnBaMn_2O_{5.5}$ intermediate phase, J. Mater. Chem. A 4 (2016) 11635.

[7] A.A. Taskin, Yoichi Ando, Peculiar ferrimagnetism associated with charge order in layered perovskite $GdBaMn_2O_{5.0}$, Phys. Rev. Lett. 98 (2007) 207201.

[8] S. Berri, N. Bouarissa, M. Attallah, First-principles predictions on half-metallic results of $RBaMn_2O_{6-\delta}$ (R=Nd, Pr, La and δ =0, 1) double perovskite compounds, J. Supercond. Nov. Magn. 33 (2020) 1737.

[9] S.V. Trukhanov, V.A. Khomchenko, L.S. Lobanovski, M.V. Bushinsky, D.V. Karpinsky, V.V. Fedotova, I.O. Troyanchuk, A.V. Trukhanov, S.G. Stepin, R. Szymczak, C.E. Botez, A. Adair, Crystal structure and magnetic properties of ba-ordered manganites $Ln_{0.70}Ba_{0.30}MnO_{3-\delta}$ (Ln=Pr, Nd), J. Exp. Theor. Phys. 103 (2006) 398.

[10] I.O. Troyanchuk, S.V. Trukhanov, G. Szymczak, New family of $LnBaMn_2O_{6-\delta}$ manganites (Ln=Nd, Sm, and Gd), Crystallogr. Rep. 47 (2002) 658.

[11] Thibault Broux, Mona Bahout, James M. Hanlon, Olivier Hernandez, Serge Paofai, Andrey Berenov, Stephen J. Skinner, High temperature structural stability, electrical properties and chemical reactivity of $NdBaCo_{2-x}Mn_xO_{5+\delta}$ ($0 \le x \le 2$) for use as cathodes in solid oxide fuel cells, J. Mater. Chem. A 2 (2014) 17015.

[12] Konrad Świerczek, Alicja Klimkowicz, Kun Zheng, Bogdan Dabrowski, Synthesis, crystal structure and electrical properties of *A*-site cation ordered $BaErMn_2O_5$ and $BaErMn_2O_6$, J. Solid State Chem. 203 (2013) 68.

[13] Tomohiko Nakajima, Hideki Yoshizawa, Yutaka Ueda, *A*-Site randomness effect on structural and physical properties of ba-based perovskite manganites, J. Phys. Soc. Japan 73 (2004) 2283.

[14] Tomohiko Nakajima, Hiroshi Kageyama, Hideki Yoshizawa, Kenji Ohoyama, Yutaka Ueda, Ground state properties of the *A*-site ordered manganites, $RBaMn_2O_6$ (R = La, Pr and Nd), J. Phys. Soc. Japan 72 (2003) 3237.

[15] D. Akahoshi, M. Uchida, Y. Tomioka, T. Arima, Y. Matsui, Y. Tokura, Random potential effect near the bicritical region in perovskite manganites as revealed by comparison with the ordered perovskite analogs, Phys. Rev. Lett. 90 (2003) 177203.

[16] Florent Tonus, Mona Bahout, Vincent Dorcet, Rakesh K. Sharma, Elisabeth Djurado, Serge Paofai, Ronald I. Smith, Stephen J. Skinner, A-site order–disorder in the $NdBaMn_2O_{5+\delta}$ SOFC electrode material monitored in situ by neutron diffraction under hydrogen flow, J. Mater. Chem. A 5 (2017) 11078.

[17] Aisha Khatun, Payel Aich, Alexander Schoekel, Andrei Gloskovskii, Soumyakanta Panda, Niharika Mohapatra, Subhendra D. Mahanti, U. Manju, D. Topwal, Intertwined crystal structure, magnetic, and charge transport properties in mixed valent *A*-site ordered manganite $NdBaMn_2O_6$, J. Alloys Compd. 988 (2024) 174205.

[18] B. Sudakshina, M.V. Suneesh, B. Arun, D. Chandrasekhar Kakarla, M. Vasundhara, Effects of Cr,Co,Ni substitution at Mn-site on structural, magnetic properties and critical behaviour in $Nd_{0.67}Ba_{0.33}MnO_3$ mixed-valent manganite, J. Magn. Magn. Mater. 548 (2022) 168980.

[19] S. Yamada, H. Sagayama, K. Higuchi, T. Sasaki, K. Sugimoto, T. Arima, Physical properties and crystal structure analysis of double-perovskite $NdBaMn_2O_6$ by using single crystals, Phys. Rev. B 95 (2017) 035101.

[20] Md Shafiqul Islam, Daisuke Morikawa, Shigeki Yamada, Bikas Aryal, Kenji Tsuda, Masami Terauchi, Space group determination and first-principles structure optimization of the *A*-site ordered perovskite-type manganite $NdBaMn_2O_6$, Phys. Rev. B 105 (2022) 174114.

[21] Md Shafiqul Islam, Daisuke Morikawa, Shigeki Yamada, Bikas Aryal, Kenji Tsuda, Masami Terauchi, Determination of the crystal structures of $NdBaMn_2O_6$: Coexisting polar and nonpolar phases, Phys. Rev. B 108 (2023) L060104.

[22] Elena V. Mostovshchikova, Evgenii V. Sterkhov, Sergey V. Naumov, Nikita S. Ermolov, Sergey A. Uporov, Svetlana G. Titova, Effect of A-site ordering on IR absorption and magnetotransmission in $PrBaMn_2O_6$ double manganite, J. Magn. Magn. Mater. 538 (2021) 168247.

[23] Aisha Khatun, Payel Aich, Alexander Schoekel, Soumyakanta Panda, N. Mohapatra, Ashis Kumar Nandy, Subhendra D. Mahanti, D. Topwal, Variation of structural and magnetic properties of mixed-valent manganites through A-site cationic ordering, J. Magn. Magn. Mater. 568 (2023) 170367.

[24] A.C. Larson, R.B. Von Dreele, General Structure Analysis System - GSAS/EXPGUI, Los Alamos National Laboratory Report No. LAUR 86-748, 2000;
B.H. Toby, *EXPGUI*, a graphical user interface for *GSAS*, J. Appl. Crystallogr. 34 (2001) 210.

[25] C. Macchiutti, J.R. Jesus, F.B. Carneiro, L. Bufaiçal, M. Ciomaga Hatnean, G. Balakrishnan, E.M. Bittar, Absence of zero-field-cooled exchange bias effect in single crystalline $La_{2-x}A_xCoMnO_6$ (A=Ca,Sr) compounds, Phys. Rev. Mater. 5 (2021) 094402.

[26] E.V. Mostovshchikova, E.V. Sterkhov, S.V. Pryanichnikov, S.G. Titova, IR magnetotransmission in double manganite $NdBaMn_2O_6$ with different degrees of order in A-position, Bull. Russ. Acad. Sci. Phys. 88 (2024) 555.

[27] E. Suard, F. Fauth, C. Martin, A. Maignan, F. Millange, L. Keller, Role of the A-site cations on the magnetic structures and transport properties in the $Nd_{0.7}Ba_{0.3-y}Sr_yMnO_3$ ($0 \le y \le 0.2$) perovskite, J. Magn. Magn. Mater. 264 (2003) 221.

[28] I.A. Abdel-Latif, A.M. Ahmed, H.F. Mohamed, S.A. Saleh, J.A. Paixão, Kh.A. Ziq, M.Kh. Hamad, E.G. Al-Naharif, M. Ghozza, S. Allam, Magne- tocaloric effect, electric, and dielectric properties of $Nd_{0.6}Sr_{0.4}Mn_xCo_{1-x}O_3$ composites, J. Magn. Magn. Mater. 457 (2018) 126–134.

[29] F. Millange, E. Suard, V. Caignaert, B. Raveau, $YBaMn_2O_5$: crystal and magnetic structure reinvestigation, Mater. Res. Bull. 34 (1999) 1.

[30] J. Blasco, J.A. Rodríguez-Velamazán, G. Subías, M.C. Sánchez, J.L. García-Muñoz, Magnetic order and magnetic properties of the oxygen deficient $SmBaMn_2O_5$ layered perovskite, Mater. Res. Bull. 150 (2022) 111780.

[31] V. Caignaert, F. Millange, B. Domengès, B. Raveau, A new ordered oxygen-deficient manganite perovskite: $LaBaMn_2O_{5.5}$. Crystal and magnetic structure, Chem. Mater. 11 (1999) 930.

[32] J.B. Goodenough, Magnetism and chemical bond, Interscience (1966).

[33] R.D. Shannon, Revised effective ionic radii and systematic studies of interatomic distances in halides and chalcogenides, Acta Cryst. A 32 (1976) 751.

[34] N.W. Ashcroft, N.D. Mermin, Solid State Physics, Cengage Learning, New York, 2011.

[35] V.V. Parfenov, Sh. Sh. Bashkirov, I.A. Abdel'-Latif, A.V. Marasinskaya, Transfer phenomena in $Nd_{0.65}Sr_{0.35}Mn_{1-x}Fe_xO_3$ ferrimanganites, Russ. Phys. J. 46 (2003) 10.

[36] S. Mugiraneza, A.M. Hallas, Tutorial: a beginner's guide to interpreting magnetic susceptibility data with the Curie–Weiss law, Commun. Phys. 5 (2022) 95.

[37] A.-M. Haghiri-Gosnet, J.-P. Renard, CMR manganites: physics, thin films and devices, J. Phys. D: Appl. Phys. 36 (2003) R127.